Pulse shape discrimination characteristics of stilbene crystal, pure and ^{6}Li loaded plastic scintillators for a high resolution coded-aperture neutron imager

Michal J. Cieslak*[1], Kelum A.A. Gamage[1], and Robert Glover[2]

[1] *Department of Engineering, Lancaster University, Lancaster LA1 4YW, UK*
[2] *Radiometric Systems Group, Sellafield Ltd, Seascale CA20 1PG, UK*

30th June 2017

Abstract

Pulse shape discrimination performances of single stilbene crystal, pure plastic and ^{6}Li loaded plastic scintillators have been compared. Three pulse shape discrimination algorithms have been tested for each scintillator sample, assessing their quality of neutron/gamma separation. Additionally, the digital implementation feasibility of each algorithm in a real-time embedded system was evaluated. Considering the pixelated architecture of the coded-aperture imaging system, a reliable method of simultaneous multi-channel neutron/gamma discrimination was sought, accounting for the short data analysis window available for each individual channel. In this study, each scintillator sample was irradiated with a ^{252}Cf neutron source and a bespoke digitiser system was used to collect the data allowing detailed offline examination of the sampled pulses. The figure-of-merit was utilised to compare the discrimination quality of the collected events with respect to various discrimination algorithms. Single stilbene crystal presents superior neutron/gamma separation performance when compared to the plastic scintillator samples.

1 Introduction

Pulse shape discrimination (PSD) is a well-established method of separating fast neutron and gamma-ray interactions within an organic scintillation medium. The method is based on the difference in the decay time of fluorescence emitted within an organic scintillator as a result of an interaction between the ionising particle and the scintillant. The fluorescence decay time observed for heavy ionising particles, such as protons, is longer when compared to electrons [1]. Fast neutrons and gamma-ray photons interact with an organic scintillant predominantly through elastic scattering with a proton and Compton scattering, respectively. Consequently, the fluorescence decay rate exhibited by recoil protons and recoil electrons (Compton scattering) can be compared to infer the origin of the interaction [2].

Fluorescence emission is linked to the kinetic energy of the incoming particle. When it interacts with the organic molecules, the particle excites π-electrons within the structure of the scintillation medium [2]. Thus, the π-electrons are raised to one of the exited electronic states. Depending on the initial energy of the radiating particle, it can be lifted to a singlet S_S or triplet T_S state. Prompt fluorescence (also known as *fast component* of the scintillation process) is emitted when the particle in the S_S state returns to the ground electronic state. The lifetime of a S_S state is measured in nanoseconds and is short when compared to that of a T_S state, which can be up to 1 millisecond. The longer de-excitation time of the T_S state is often associated with the π-electron transferring to one of S_S states before returning to the ground state. Hence, fluorescence emission is delayed resulting in the occurrence of the *slow component* of the scintillation process.

The fraction of light in the *slow component* of the scintillation can be used to infer the origin of the interacting particle. The decay rate of the *slow component* varies for the incoming particles of

*m.cieslak@lancaster.ac.uk

different nature but equal kinetic energy. When heavy particles interact with the scintillation medium, they demonstrate greater rate of energy loss. Therefore, the fluorescence decay time of recoil protons (resulting from neutron interactions) is longer when compared to the fluorescence decay time of recoil electrons (resulting from gamma-ray photon interactions) [2]. Thus, the difference in the fluorescence decay rate forms a basis for neutron/gamma PSD techniques in organic scintillators. Fluorescence decay characteristics for a theoretical neutron and a gamma-ray are shown in Fig. 1. Various PSD techniques have been developed in analogue and digital domains to separate neutron events from gamma-rays effectively and efficiently.

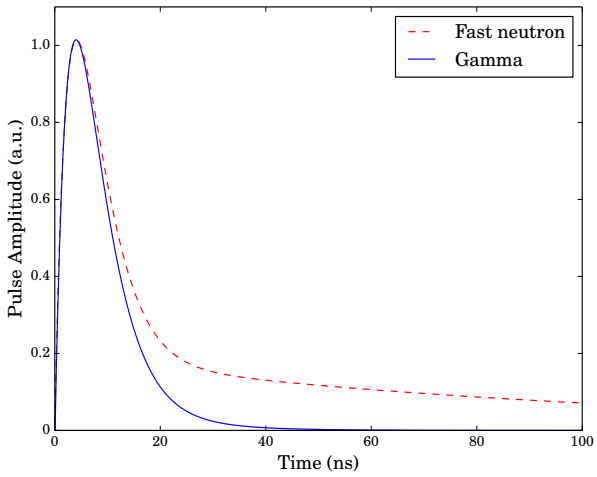

.

Figure 1: Theoretical fast neutron and gamma-ray scintillation pulses induced in an organic solid scintillation medium based on the information from Knoll [2] and Zaitseva et al. [3]

When the research into neutron/gamma discrimination was at its origins, the techniques developed were intended for liquid scintillator detectors [1, 2, 4, 5]. As a result, many liquid scintillators have been developed and accurately characterised [6–10]. However, due to flammable properties of some liquid scintillators and their susceptibility to leaks, these were not suitable for many industrial applications. An alternative in a form of solid scintillation detectors was perceived inferior to liquid counterparts with regards to neutron/gamma separation (plastic scintillators) and light output (organic crystals) [2]. Recent progress into techniques of developing solid organic scintillators shows that their PSD performance improved significantly, with stilbene crystal aspiring to outperform widely used EJ-309 liquid scintillator [11–16]. Hence, only solid scintillation samples were selected for testing.

In this paper, a succinct review of selected PSD methods is presented, aiming to identify the most suitable candidate for a real-time scintillation based coded-aperture neutron imaging system. Three chosen techniques are then experimentally tested and the results compared for three different scintillator types. Additionally, performance assessment of the PSD method and scintillator combinations was examined. Online data processing was adopted in this study for the investigation of the three selected methods. Computational complexity of each method was also considered with regards to the real-time operation feasibility. A brief review of the existing organic scintillator characterisation methods, which was performed prior to the characterisation work undertaken in this study, is also presented.

2 Pulse shape discrimination methods in organic scintillators

2.1 Analogue PSD methods

Discovery of the pulse shape variation between neutron and gamma-ray induced incidents triggered a long search for the most effective separation method. Around the time of its discovery, PSD was dominated by two algorithms implemented in the analogue domain: zero-crossing and charge comparison method

(CCM). The former method transforms the photo-detector output pulse into bipolar signal. The time between the trigger and the zero-crossing point is then used as benchmark for neutron and gamma discrimination [17]. Although less often used nowadays, mainly due to the implementation practicality of the digital approaches, the zero-crossing method shows very good PSD performance when implemented in organic scintillator studies [18, 19].

The latter method is based on the ratio between the charge integrated over the duration of the entire pulse (*long integral*) and the charge integrated over the tail of the pulse (*short integral*). Analogue CCM (also known as charge integration method) was first described by Brooks and utilised various RC circuit combinations to perform the integration of the entire pulse and its tail [1]. A comprehensive investigation of these two analogue methods has been performed by Nakhostin [17].

2.2 Digital Charge Comparison Method

The advent of digital electronics enabled complicated analogue circuits to be replaced by a few lines of a computer code. Therefore, both analogue methods were successfully employed in the digital domain, with CCM becoming one of the most powerful PSD algorithms [20]. Recent study, which compared PSD performance of the digital CCM and the analogue zero-crossing method, reports that the estimated figure-of-merit (FOM) for the digital CCM is on average 20% greater than that obtained for the analogue zero crossing method [21]. However, similar investigation conducted over two decades earlier indicates superior performance of the zero-crossing method over the digital CCM which illustrates the progress of the digital approaches [22].

The arrival of fast high resolution analogue-to-digital converters (ADC) enabled integration to be calculated as an area under the digitised pulse. There are three integration algorithms that can be easily employed: running sum, trapezoidal rule and Simpson's rule. The running sum is the simplest algorithm, where the integral is calculated as a sum of the digitised samples. The trapezoidal rule estimates the area between two digitised samples by taking an average of the two adjacent samples, whereas the Simpson's rule approximates the integral by calculating quadratic polynomials for specific intervals. Since previous research suggests that all three integration algorithms provide identical PSD results when used in the digital CCM implementation, the running sum algorithm was used in this research [17].

2.3 Simplified Digital Charge Comparison

Different decay rates of the slow scintillation components for neutron and gamma-ray events define the separation capability of an organic scintillator. The simplified digital charge comparison (SDCC) method focuses on the period between the peak amplitude sample and the final sample of the digitised signal. As the difference in the decay rate between the gamma-ray photon and neutron induced pulses can be observed some time after the peak, an interval was identified when the difference is most prominent [23]. The start sample and the end sample of the interval are defined by a and b parameters in Eq. (2.1), respectively. These parameters specify the interval of the *short integral*.

$$D = log(\sum_{n=a}^{n=b} {x_n}^2) \tag{1}$$

Generally, a parameter corresponds to three-sixteenths and b to one half of the pulse length where the peak amplitude is considered as the first sample. The discrimination parameter D is then plotted against the magnitude of the peak amplitude to separate the particles. Preceding work advocates a superior discrimination performance of this method in comparison to other digital discrimination algorithms [24].

2.4 Pulse Gradient Analysis

Digital signal processing, implemented using advanced field-programmable gate arrays (FPGA) and high sampling rate ADCs, provided a way of performing PSD faster than it was ever possible in the analogue domain. However, the aforementioned CCM and SDCC algorithms require the whole pulse to be digitised before the discrimination can be performed. Pulse Gradient Analysis (PGA) can be performed with only two samples taken at the early stages of a scintillation pulse [26]. The magnitudes of the *peak amplitude* and the sample amplitude (known as the *discrimination amplitude*), recorded a specific time period after

the peak amplitude, are plotted against each other to separate neutrons from gamma-rays. Since only the magnitudes of the specific samples are considered the discrimination process can be completed faster in comparison to other methods. Hence, this method was successfully implemented in a multi-channel real-time Mixed Field Analyser (MFA) [27].

2.5 Other Pulse Shape Discrimination methods

There exist other digital discrimination methods implemented in the time and frequency domains [28]. Generally, methods not mentioned in the previous sections require more complex and resources-exhausting analysis of the digitised pulses. Some algorithms, such as Neutron Gamma Model Analysis (NGMA), compare digitised signals with neutron and gamma pulses modelled prior to the analysis [24]. Such methods are not desirable for a high resolution real-time neutron imaging system where the discrimination results are to be fed to an image reconstruction algorithm.

3 Existing characterisation techniques of organic scintillation detectors

3.1 Digitiser selection

The digital CCM is one of the most powerful and hence has become one of the most often utilised neutron/photon separation methods in organic scintillator characterisation studies. Due to clear advantages of the digital methods over the analogue counterparts, such as implementation practicality and performance superiority [21], the latter are only rarely used. Thus, an appropriate digitiser must be selected, so that the information contained in the analogue signal is truthfully transferred into the digital domain. Generally, the higher the sampling rate and the resolution of the digitiser's ADC, the more accurate the representation of the analogue signal. However, the ADC's resolution normally decreases as the sampling rate increases.

Previous study performed by Flaska et al. [29] reports that at least 250 MHz sampling frequency is required to obtain good PSD results. Nonetheless, another study, conducted two years after the study by Flaska, successfully carried out crystal scintillator characterisation using 14-bit resolution, 200 MSps digitiser [13]. A digitiser of equal resolution and even lower sampling frequency (150 MSps) was effectively utilised to perform PSD for a neutron survey meter [30].

3.2 Performance assessment methods of organic scintillators

With the light output of the scintillator detector adequately represented in the digital domain, further analysis of the pulse shape can be performed. Since liquid PSD scintillation detectors have become a preferred choice in many nuclear facilities, there exist various performance assessment criteria which can be easily adopted for solid organic scintillators. Furthermore, with the continuous development of the new solid organic scintillation materials, they are often contrasted with liquid organic scintillators [16,31].

The most important characteristic of any PSD scintillator is the FOM. It is utilised to compare the separation quality, based on the number of detected particles of different types. The FOM can be obtained by plotting a histogram of the ratio of the maximum and the minimum amplitudes of the digitised pulses [2,28]. Another approach exploits the concept of discrimination line where the histogram is plotted as a function of the orthogonal distance from each particle to the discrimination line [24].

A decent quality PSD with a sufficiently good FOM enables further analysis of the identified particles. Based on the number of neutron events and gamma-ray photons accepted by the digitiser system, it may be feasible to identify the differences between radioactive isotopes detected [32]. One of such methods is R-factor, which computes the ratio of neutron and gamma-ray interactions within the scintillator. The FOM, as well as the R-factor, are described in detail in the following sections. These characteristics are used to perform quality assessment of the chosen samples with regards to PSD.

4 Experimental method

Three different organic solid scintillator samples were in turn irradiated with ^{252}Cf (half-life of 2.64 years) source located at Lancaster University, Lancaster, UK. A pure PSD plastic scintillator sample (25 mm diameter, 25 mm thick) and a ^{6}Li loaded PSD plastic scintillator sample (40 mm diameter, 25 mm thick) were both provided by the Lawrence Livermore Laboratory (LLNL), USA - denoted by the LLNL numbers 5706 and 9023, respectively. A single stilbene crystal (20 mm diameter, 20 mm thick) was obtained from Inrad Optics [33]. The experimental set-up is shown in Fig. 2 where the radioactive source was in a water tank. The detector front was placed 15 cm away from the source and 10 cm away from Pb shielding. The Pb shielding was utilised to reduce the number of gamma-rays reaching the scintillator detector.

The back of each scintillator sample was covered with EJ-510 reflective coating. Each sample was then coupled to an ET Enterprises 9107B photomultiplier tube (PMT) with EJ-550 silicone grease, used to maximise the light transmission properties between scintillator and the PMT. The PMT was supplied in a B2/RFI housing with a 637BFP tapered distribution voltage divider. The PMT module supplied by ET Enterprises was enclosed in a light-proof tube. Depending on the scintillator type, the positive high voltage supply connected to the cathode of the PMT was varied between 850 V and 900 V. The PMT anode was connected to a bespoke digitiser system which utilises a Analog Devices AD9254 150 MSps, 14-bit amplitude resolution ADC directly linked to a Altera Cyclone IV EP4CE115 FPGA. The system recorded 28 raw samples (taken approximately every 6.67 ns) per each triggered pulse. The registered data were transferred to a laptop running Linux via universal asynchronous receiver/transmitter (UART) configured to transfer data at 8 Mbits/s. The received data were further processed by a bespoke script developed in Python.

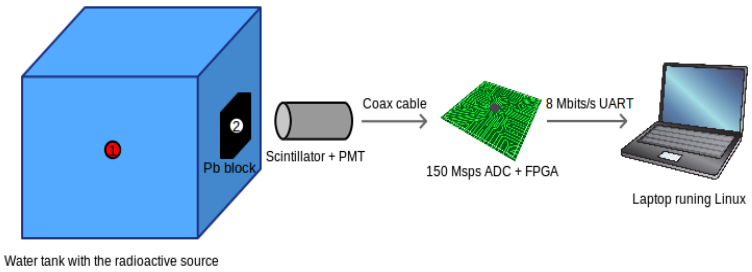

Figure 2: Schematic diagram of the experimental set-up. ^{252}Cf source is in the centre of a water-filled metal tank (position 1). During the experiments the source is moved to the edge of the tank (position 2).

5 Results

Prior to PSD implementation each digitised pulse was run through a bespoke pulse pile-up rejection algorithm. The algorithm simply rejected any pulse where two peaks were detected. Since each scintillator sample was exposed to ^{252}Cf neutron field for approximately 1 hour, many thousands of pulses were collected, with the number of pulses accepted by the pulse pile-up rejection algorithm varying between approximately 60,000 and 80,000 pulses for the three samples tested.

Reconstructed analogue pulses are often affected by high frequency noise, which may lead to misclassification of a pulse when PSD is performed. Moving average filter was applied to each digitised pulse to smooth out the high frequency component [24]. Given the relatively low number of recorded samples per triggered pulse, a 7-point moving average filter was used with the digitised input samples placed symmetrically around the filtered output point. Thus, each filtered sample is replaced with an average, which leads to the 'raw' digitised samples being lost in the computation. Although the filter removes the

'raw' components from the signal to be discriminated, reduction in the high frequency components in the processed signal results in lower neutron/gamma misclassification probability [25]. Following that, PSD was performed on each pulse using the methods specified earlier. For each method implemented, the neutron and the gamma-ray plumes were separated using a discrimination line (where possible) [34]. In each case, shown in Fig. 3 to Fig. 5, plume above the discrimination line is corresponding to neutrons and the plume below the line to gamma-rays.

Based on PSD results obtained for each scintillator sample, FOM was calculated (using Eq. 5.1) to compare their performance in particle separation. *Peak separation* in Eq. (5.1) represents the difference between the peak distances from a normal distribution fitting of neutron and gamma-ray plumes; FWHM is the full-width at half-maximum for each particle distribution. Further, Eq. (5.2) was utilised to calculate R-factor values. The R-factor is a ratio of the number of gamma-rays over the number of neutrons which is often utilised to quantify the gamma-ray rejection efficiency in neutron detectors. Results are presented in Table 1. where Poisson approximation of the distribution was assumed to determine the corresponding uncertainty.

$$FOM = \frac{Peak\ separation}{FWHM_g + FWHM_n} \tag{2}$$

$$R = \frac{\sum_g}{\sum_n} \tag{3}$$

5.1 CCM implemented in the digital domain

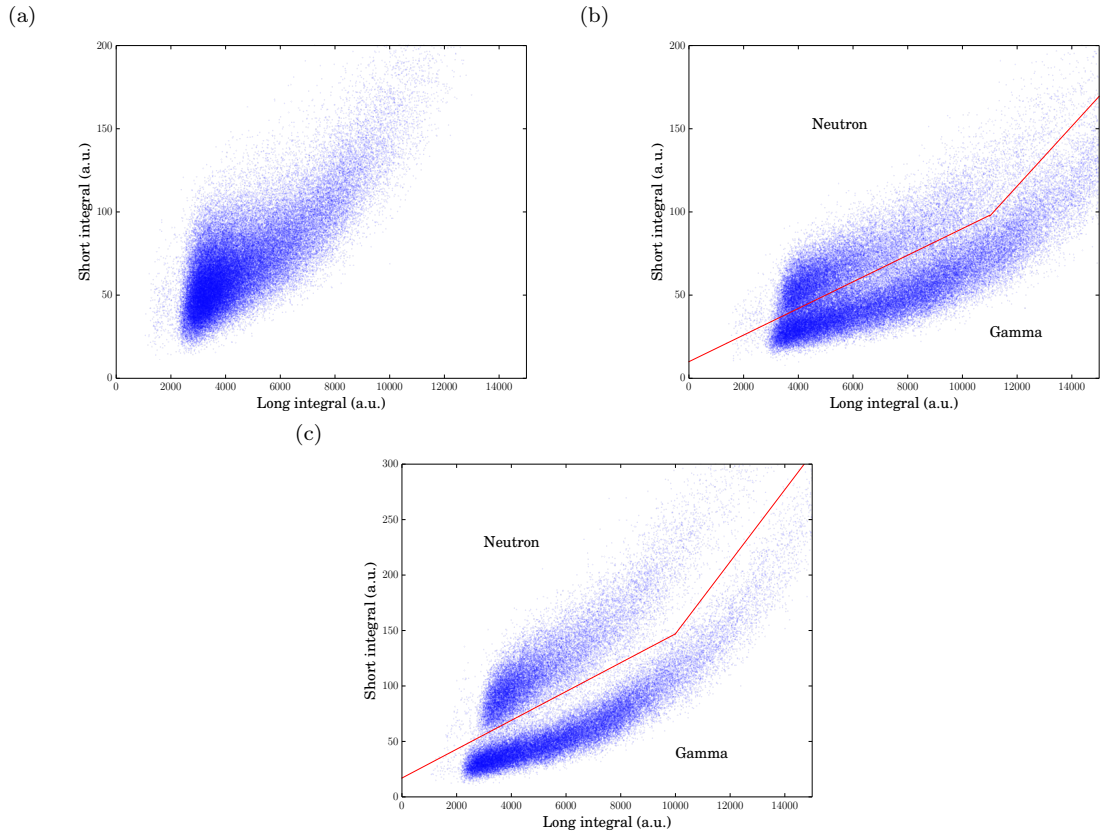

Figure 3: PSD discrimination plots using CCM method: (a) ^{6}Li loaded plastic scintillator, (b) Plastic scintillator and (c) Single stilbene crystal.

Scatter plots of the *short integral* against the *long integral* for the three samples are shown in Fig. 3. There is no discrimination line plotted for ^{6}Li loaded plastic scintillator sample, as there is no clear

separation between fast neutrons and gamma-ray photons when irradiated with ^{252}Cf radioactive source. Hence, it was not possible to estimate the FOM for this scintillator sample. Estimated FOM values for the plastic scintillator sample and single stilbene crystal were 0.649 and 0.867, respectively. It can be clearly noticed that the stilbene crystal presents superior PSD performance when compared to the two plastic scintillation samples tested.

5.2 SDCC implemented in the digital domain

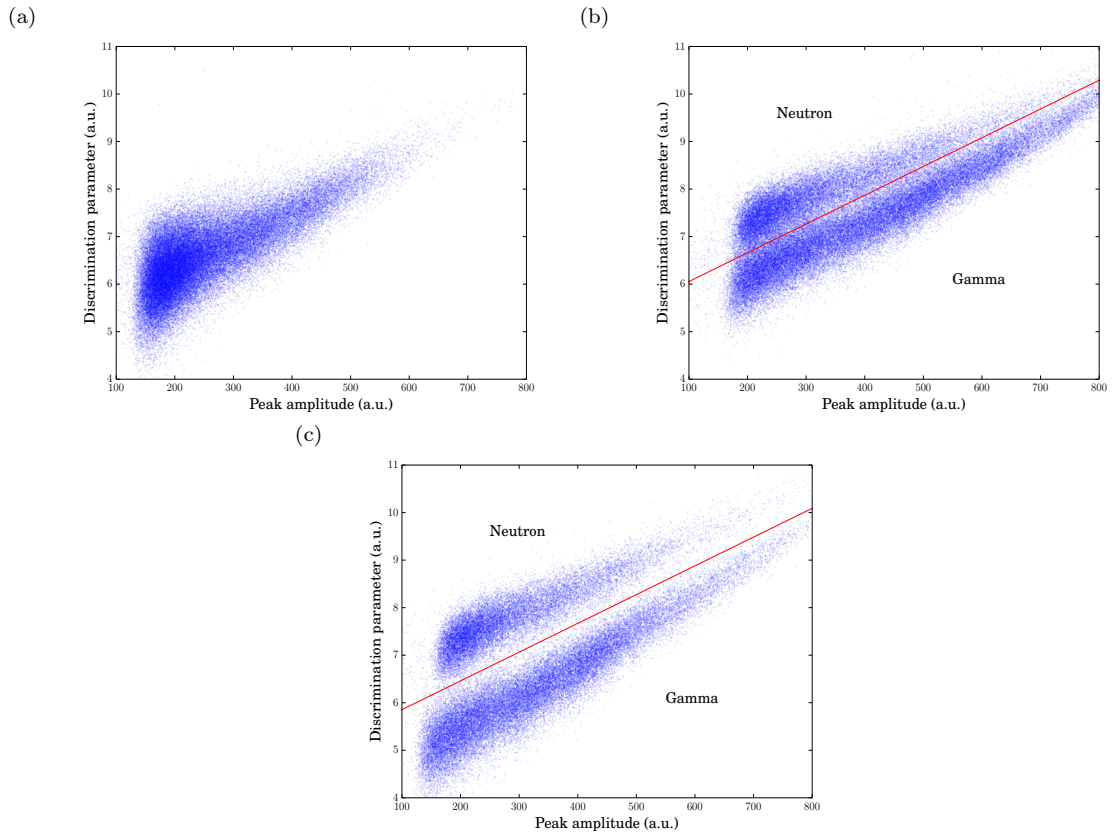

Figure 4: PSD discrimination plots using SDCC method: (a) ^{6}Li loaded plastic scintillator, (b) Plastic scintillator and (c) Single stilbene crystal.

Fig. 4. shows scatter plots of PSD performed using SDDC method; in this case discrimination parameter D is plotted versus the peak amplitude. The results obtained show similar characteristics to those obtained with CCM algorithm. The FOM value for single stilbene crystal estimated at 1.033 was far higher than 0.761 obtained for the plastic scintillator sample. Similarly to the results of the PSD using CCM algorithm, SDDC method was also unsuccessful in discriminating between fast neutron events and gamma-ray photons in ^{6}Li loaded plastic scintillator.

5.3 PGA implemented in the digital domain

Results of PSD implemented using PGA method are shown in a form of scatter plots in Fig. 5. and they are comparable to those obtained using the other two methods. In this instance *discrimination amplitude* was plotted against *peak amplitude*, with the estimated FOM values of 0.631 for the plastic scintillator sample and 0.823 for single stilbene crystal. In the same way as for the CCM and SDDC algorithms, it was not possible to draw a discrimination line between fast neutrons and gamma-rays for ^{6}Li loaded plastic scintillator.

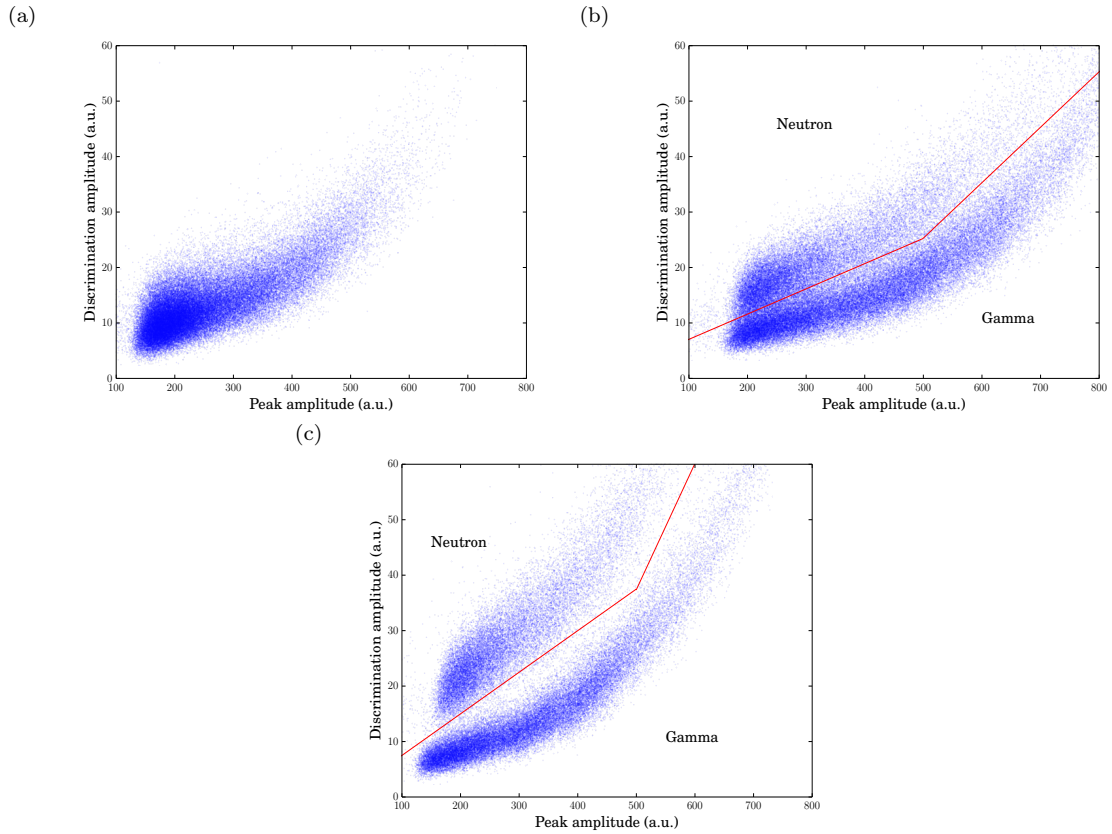

Figure 5: PSD discrimination plots using PGA method: (a) ^{6}Li loaded plastic scintillator, (b) Plastic scintillator and (c) Single stilbene crystal.

5.4 Separation quality assessment

Distribution of each point from the discrimination line plots are shown in Fig. 6. for all scintillator/PSD method combinations. The distribution plots are corresponding to the cases with the highest FOM value estimated for each of the scintillator samples. Based on the distributions presented, a good agreement can be observed across the three methods tested with regards to PSD performance of the two scintillation samples compared. Statistical analysis of the distributions shows that 95% confidence level in the results can be assumed for stilbene crystal using CCM and SDCC. The data generated for these two methods was further validated by chi-square test against the normal distribution hypothesis. It follows that 95% of the detected particles will be correctly discriminated in this specific experimental scenario.

For the remaining scintillator/PSD method combinations, a clear separation can only be observed within one standard deviation of the mean. Hence, the resulting confidence interval is considerably smaller than for the aforementioned cases. Although the stilbene PGA combination still claims reasonably good separation (approximately 90% confidence level), the plastic scintillator separation performance is significantly inferior as evidenced by the results on the left in Fig. 6. Although chi-square normality test validated the normal hypothesis for all the distribution fits considered within their respective confidence intervals, it must be noted that the test was performed against single Gaussian distributions (separately for each neutron and gamma-ray distributions). This was necessary to ensure that FWHM correctly represents the fluctuations of Gaussian distribution. Neutron and gamma-ray distribution fit lines were only plotted to the zero point (discrimination line), in order to clearly show the difference in misclassification quality between stilbene and plastic scintillator samples.

A general consistency across the three separation methods can be found, as presented in Table 1., with the single stilbene crystal providing results of supreme quality when compared to the pure plastic scintillator sample. Since there is a clearer separation between the neutron and gamma-ray normal distribution fits in Fig. 6 (b),(d) and (f) than in Fig 6 (a),(c) and (e), there is a lower chance of particle

misclassification for the single stilbene crystal than for the pure plastic scintillator.

Optimisation of the estimated FOM values was performed, as shown in Fig. 7. The length of the *short integral* was varied for CCM method by adjusting the starting sample number. Samples investigated range between sample number 4 and sample number 12, with the peak amplitude being considered as sample number 1. The optimal sample numbers for the pure plastic and the stilbene crystal scintillators were 10 and 8, as presented in Fig. 7 (a) and Fig. 7 (b), respectively. These sample numbers correspond to 66.70 and 53.36 ns after the sample of the peak amplitude. With the peak amplitude usually occurring within first 20 ns of the pulse, the shortest window inspected was approximately 86.71 ns. This specific interval was considered because outside this range no clear separation between neutron and gamma-ray plumes was observed.

The length of the *short integral* was also varied for SDCC method where the value of parameter a was adjusted. In this case the optimal values were found approximately 53.36 and 46.69 ns (sample numbers 8 and 7) after the peak amplitude for the pure plastic and stilbene crystal scintillators, respectively. Similarly to CCM algorithm, sample numbers outside the range presented in Fig. 7 (c) and Fig. 7 (d) were excluded because of the two particle plumes not being distinguishable.

The *discrimination amplitude* sample number was inspected for PGA algorithm. Since PGA method only considers magnitudes of two samples, there is no need to specify a window to be considered with reference to the *peak amplitude*. Both scintillators exhibit the optimal PSD performance when sample number 10 (occurring 66.70 ns after sample number 1) is plotted against the *peak amplitude*. The results of PGA algorithm optimisation are presented in Fig. 7 (e) and Fig. 7 (f).

Table 1: FOM and R-factor values determined for the pure plastic and stilbene crystal scintillator samples for the three PSD algorithms compared in this study.

Sample	**Method**	**gamma-rays**	**neutrons**	**FOM**	**R-factor**
Pure plastic	CCM	38790	36696	0.649 ± 0.020	1.057 ± 0.002
	SDCC	38936	37492	0.761 ± 0.004	1.038 ± 0.002
	PGA	39784	36229	0.631 ± 0.010	1.098 ± 0.002
Stilbene crystal	CCM	30747	29450	0.867 ± 0.030	1.044 ± 0.003
	SDCC	34368	26026	1.033 ± 0.005	1.321 ± 0.003
	PGA	30460	29628	0.823 ± 0.020	1.028 ± 0.003

6 Discussion

Three solid organic scintillation samples were exposed to ^{252}Cf fission source, and the collected data discriminated between neutrons and gamma-rays using three different PSD techniques. Results obtained are in general agreement across the three algorithms implemented, with single stilbene crystal showing superior neutron/gamma separation performance. All three algorithms failed to separate fast neutrons from gamma-rays within ^{6}Li loaded plastic scintillator, whereas the FOM values estimated for the pure plastic scintillator suggest relatively good discrimination performance. This difference in discrimination quality is associated with the doping of the former, which enables neutrons thermalized within the organic detector to be captured by the high neutron capture cross-section ^{6}Li.

Since the neutron energy spectrum of ^{252}Cf averages at approximately 2.1 MeV, a large number of neutrons emitted would fall below the 1 MeV threshold. Previous studies support the claim that PSD performance of organic plastic scintillators increases when exposed to higher energy neutron fields (>1 MeV). When exposed to ^{241}AmBe neutron field ^{6}Li loaded plastic sample tested in this study performed considerably better in terms of fast neutrons and gamma separation [28]. Moreover, ^{252}Cf source at Lancaster University, UK is in a water tank, where neutrons are thermalized as a result of their interaction with H atoms. It can therefore be concluded that ^{6}Li loaded plastic can be beneficial for certain applications but neutron capture events are difficult to separate from gamma-ray photons in relatively lower energy fields, such as from a moderated ^{252}Cf source, as presented in this and previous studies [28].

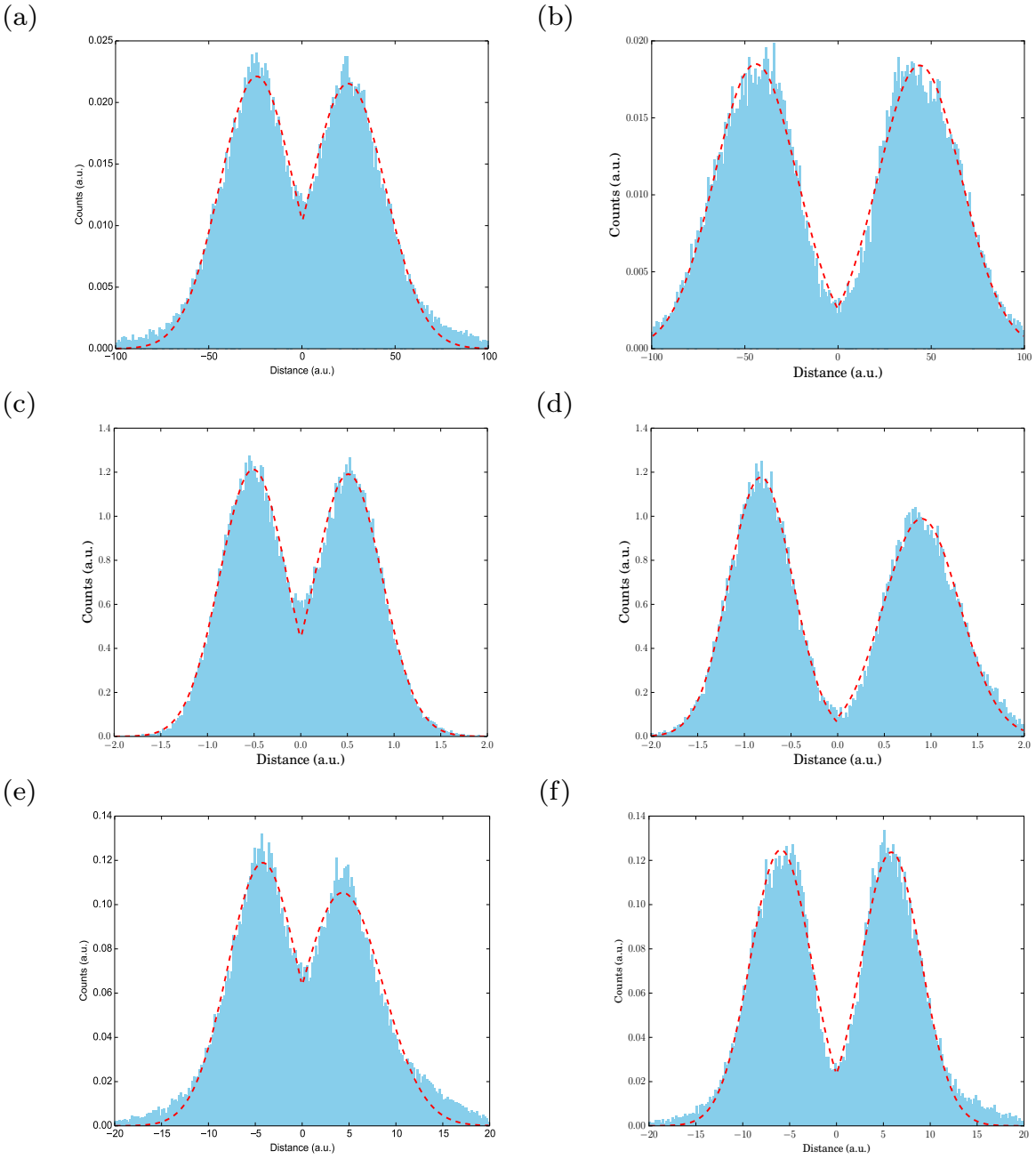

Figure 6: Distribution of each point from the discrimination line for all scintillator sample/PSD method combinations: (a) plastic CCM, (b) stilbene CCM, (c) plastic SDCC, (d) stilbene SDCC, (e) plastic PGA and (f) stilbene PGA.

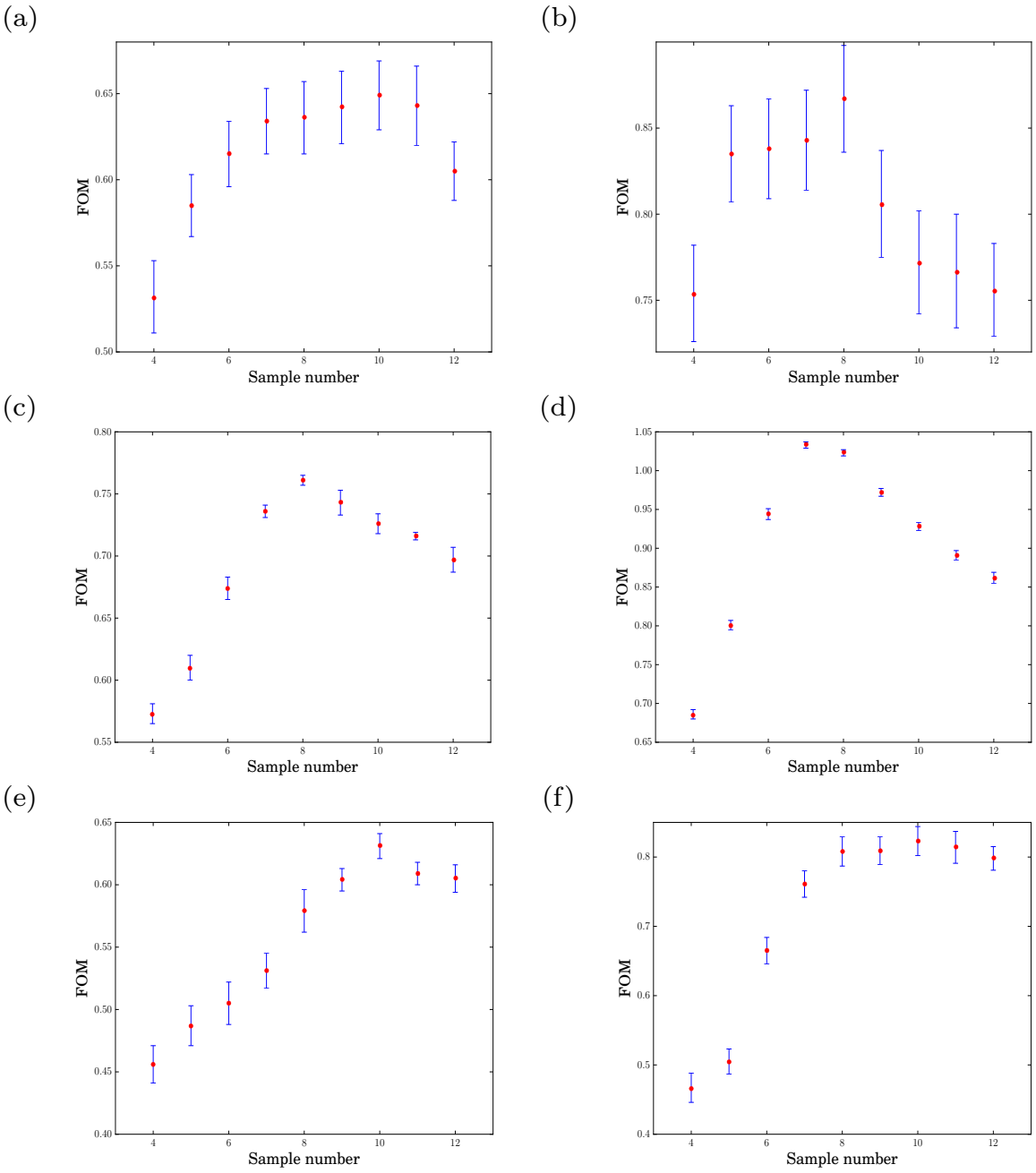

Figure 7: FOM optimisation plots for all scintillator sample/PSD method combinations: (a) plastic CCM, (b) stilbene CCM, (c) plastic SDCC, (d) stilbene SDCC, (e) plastic PGA and (f) stilbene PGA.

R-factor measurements show reasonable consistency across the algorithms tested for the two scintillator samples, where neutron events and gamma-ray photons were successfully separated. However, the average R-factor value of approximately 1.098 is lower than the expected 2.118 (based on the average number of neutrons and gamma-rays per fission event of 3.767 and 7.980, respectively [35] [36]). It is thought that the difference is associated with a Pb block, which was used to reduce the number of gamma-rays reaching the detector, placed adjacent to the water tank, as shown in Fig. 2.

One of the aims of this study was to find a suitable scintillation material for a scintillator based coded-aperture neutron imager to potentially extend the neutron detection range. A preceding study identified single stilbene crystal as a suitable solution for the imaging system [37]. The results obtained not only do support the claim of the preceding study, but also show that neutrons and gamma-ray photons can be clearly separated within the stilbene crystal. As such, stilbene crystal can be perceived as an ideal candidate from the performance point of view for applications where neutron/gamma separation is required to extend to below the 1 MeV neutron energy threshold.

The FOM values obtained for CCM and PGA algorithms are comparable, whereas the FOM values estimated for SDDC method are significantly higher. These results are resembled most clearly in the scatter graph presented in Fig. 4 (c), where the results of PSD performed using SDDC for the stilbene crystal are plotted. An evident separation between neutron and gamma-ray plumes enables a reduction in misclassification of particles which may sometimes occur in lower energy areas.

The neutron/photon misclassification problem in lower energy regions (< 1 MeV) for CCM has been thoroughly investigated. The method proposed by Polack et al. [38] enables misclassification reduction when there is a clear overlap of the neutron and gamma-ray plumes in the lower energy ranges. However, in this study there is a clear distinction between the two plumes for PSD using CCM for the stilbene crystal as shown in scatter plot in Fig. 3 (c). Therefore, no further method of plume separation was sought. While SDCC method transpired to be the most effective, it is also the most computationally exhaustive which may be of concern for real-time applications. However, continuous advancement in the FPGA technology makes this matter a less prevailing factor.

It is worth noting that a relatively low speed digitiser (i.e. 150 MSps) was used throughout this research which could contribute to the misclassification of the digitised pulses. Prior study, which investigated the influence of the sampling properties on the PSD performance, claims that 250 MHz digitiser would be a sensible choice when good PSD performance is required [29]. Nonetheless, successfully implemented PSD is consistent with the claim of the preceding work where the same digitiser was tested with simulated neutron and gamma-ray pulses [39]. The digitiser was also utilised in a novel neutron survey meter, which further advocates the statement that good PSD results can be obtained with 150 MSps system [30].

7 Conclusion

As evidenced by the results of the three PSD methods, single stilbene crystal outperforms the plastic scintillators when neutron/gamma separation capabilities are considered. In spite of that, relatively large machining costs and fragility of stilbene (in comparison with plastics) hinder widespread adaptation of the single stilbene crystal scintillator in nuclear decommissioning applications. Plastic scintillators on the other hand, such as EJ-299-34 from Eljen Technology, are easily machined to build scintillator arrays as required for the coded-aperture imaging system described [40].

Although SDCC method exhibits the best FOM out of the three methods tested, its computational overhead, tested using online processing, may be too high for a real-time application. PGA method offers the fastest response out of the three algorithms tested. However, its estimated FOM is the lowest. Moreover, since it only considers values of the digitised pulse at two separate points, part of the information contained may be missed. This information may be crucial when the system is required to operate in multi-channel configuration, due to the levels of high frequency noise expected. Despite the highest error associated with its FOM results of neutron/gamma separation, using CCM presents a good compromise between the digital implementation difficulty and PSD performance for the application described in the paper.

Three digital methods were employed to compare neutron/gamma discrimination performance of the chosen solid organic scintillators. Observed consistency in PSD quality for the three methods tested can be discerned as a cross validation of the test dataset collected in this study. Furthermore, the

results obtained in this work are consistent with the previous studies conducted with similar organic solid scintillators [11, 31]. Hence, it can be surmised with a sufficient level of confidence that the results obtained represent a valid PSD performance of the tested samples.

Acknowledgements

The authors would like to express thanks to Dr Natalia Zaitseva and the team at LLNL for providing the plastic scintillator samples. The authors would like to acknowledge the funding support from EPSRC (grant number EP/M507891/1) via Faculty of Science and Technology, Lancaster University, UK and Sellafield Ltd., UK. We also acknowledge the help and advice of Dr Matthew Balmer at Lancaster University, UK. The authors acknowledge the use of the package Matplotlib for all plots in this research [41].

References

[1] F. Brooks, A scintillation counter with neutron and gamma-ray discriminators, Nuclear Instruments and Methods 4 (3) (1959) 151 – 163. doi:10.1016/0029-554X(59)90067-9.

[2] G. F. Knoll, Radiation Detection and Measurement, 4th Edition, John Wiley & Sons, Hoboken, 2010.

[3] N. Zaitseva, A. Glenn, H. P. Martinez, L. Carman, I. Pawełczak, M. Faust, S. Payne, Pulse shape discrimination with lithium-containing organic scintillators, Nuclear Instruments and Methods in Physics Research Section A: Accelerators, Spectrometers, Detectors and Associated Equipment 729 (2013) 747–754. doi:10.1016/j.nima.2013.08.048.

[4] T. Alexander, F. Goulding, An amplitude-insensitive system that distinguishes pulses of different shapes, Nuclear Instruments and Methods 13 (1961) 244 – 246. doi:10.1016/0029-554X(61)90198-7.

[5] J. Adams, G. White, A versatile pulse shape discriminator for charged particle separation and its application to fast neutron time-of-flight spectroscopy, Nuclear Instruments and Methods 156 (3) (1978) 459 – 476. doi:10.1016/0029-554X(78)90746-2.

[6] H. Klein, Neutron spectrometry in mixed fields: Ne213/bc501a liquid scintillation spectrometers, Radiation Protection Dosimetry 107 (1-3) (2003) 95–109.

[7] J. Iwanowska, L. Swiderski, M. Moszynski, Liquid scintillators and composites in fast neutron detection, Journal of Instrumentation 7 (04) (2012) C04004. doi:10.1088/1748-0221/7/04/C04004.

[8] L. Stevanato, D. Cester, G. Nebbia, G. Viesti, Neutron detection in a high gamma-ray background with ej-301 and ej-309 liquid scintillators, Nuclear Instruments and Methods in Physics Research Section A: Accelerators, Spectrometers, Detectors and Associated Equipment 690 (2012) 96 – 101. doi:10.1016/j.nima.2012.06.047.

[9] C. Bass, E. Beise, H. Breuer, C. Heimbach, T. Langford, J. Nico, Characterization of a 6li-loaded liquid organic scintillator for fast neutron spectrometry and thermal neutron detection, Applied Radiation and Isotopes 77 (2013) 130 – 138. doi:10.1016/j.apradiso.2013.03.053.

[10] A. Tomanin, J. Paepen, P. Schillebeeckx, R. Wynants, R. Nolte, A. Lavietes, Characterization of a cubic ej-309 liquid scintillator detector, Nuclear Instruments and Methods in Physics Research Section A: Accelerators, Spectrometers, Detectors and Associated Equipment 756 (2014) 45 – 54. doi:10.1016/j.nima.2014.03.028.

[11] N. Zaitseva, B. L. Rupert, I. Pawełczak, A. Glenn, H. P. Martinez, L. Carman, M. Faust, N. Cherepy, S. Payne, Plastic scintillators with efficient neutron/gamma pulse shape discrimination, Nuclear Instruments and Methods in Physics Research Section A: Accelerators, Spectrometers, Detectors and Associated Equipment 668 (2012) 88–93. doi:10.1016/j.nima.2011.11.071.

[12] P. Hausladen, The Deployable Fast-Neutron Coded- Aperture Imager : Demonstration of Locating One or More Sources in Three Dimensions, 2013. info.ornl.gov/sites/publications/Files/Pub44511.pdf.

[13] N. Zaitseva, A. Glenn, L. Carman, H. Paul Martinez, R. Hatarik, H. Klapper, S. Payne, Scintillation properties of solution-grown trans-stilbene single crystals, Nuclear Instruments and Methods in Physics Research Section A: Accelerators, Spectrometers, Detectors and Associated Equipment 789 (2015) 8–15. doi:10.1016/j.nima.2015.03.090.

[14] B. Fraboni, A. Fraleoni-Morgera, N. Zaitseva, Ionizing radiation detectors based on solution-grown organic single crystals, Advanced Functional Materials 26 (14) (2016) 2276–2291. doi:10.1002/adfm.201502669.

[15] M. Gerling, P. Marleau, J. Goldsmith, Comparison of Stilbene neutron detection performance to EJ-309 (2014).

[16] M. M. Bourne, S. D. Clarke, N. Adamowicz, S. A. Pozzi, N. Zaitseva, L. Carman, Nuclear Instruments and Methods in Physics Research A Neutron detection in a high-gamma fi eld using solution-grown stilbene, Nuclear Inst. and Methods in Physics Research, A 806 (2016) 348–355. doi:10.1016/j.nima.2015.10.025.

[17] M. Nakhostin, Recursive algorithms for digital implementation of neutron/gamma discrimination in liquid scintillation detectors, Nuclear Instruments and Methods in Physics Research Section A: Accelerators, Spectrometers, Detectors and Associated Equipment 672 (2012) 1 – 5. doi:10.1016/j.nima.2011.12.113.

[18] J. Iwanowska-Hanke, M. Moszynski, L. Swiderski, P. Sibczynski, T. Krakowski, N. Zaitseva, I. A. Pawelczak, P. Martinez, A. Gektin, P. N. Zhmurin, Comparison of various plastic scintillators with pulse shape discrimination (PSD) capabilities based on polystyrene (PS), IEEE Nuclear Science Symposium Conference Record (2013) 1–3. doi:10.1109/NSSMIC.2013.6829468.

[19] M. Grodzicka, T. Szczesniak, M. Moszynski, D. Wolski, L. Swiderski, K. Grodzicki, S. Korolczuk, J. Baszak, P. Schotanus, Study of n-g discrimination by zero-crossing method with SiPM based scintillation detectors, 2014 IEEE Nuclear Science Symposium and Medical Imaging Conference, NSS/MIC 2014 (2016) 14–16. doi:10.1109/NSSMIC.2014.7431176.

[20] T. Szczęśmak, M. Grodzicka, M. Moszyński, D. Wolski, L. Swiderski, M. Szawłowski, P. Schotanus, Digital neutron-gamma discrimination methods: Charge comparison versus zero-crossing, in: 2014 IEEE Nuclear Science Symposium and Medical Imaging Conference (NSS/MIC), 2014, pp. 1–4. doi:10.1109/NSSMIC.2014.7431222.

[21] C. S. Sosa, M. Flaska, S. A. Pozzi, Comparison of analog and digital pulse-shape-discrimination systems, Nuclear Instruments and Methods in Physics Research, Section A: Accelerators, Spectrometers, Detectors and Associated Equipment 826 (2016) 72–79. doi:10.1016/j.nima.2016.03.088.

[22] D. Wolski, M. Moszyński, T. Ludziejewski, A. Johnson, W. Klamra, S. O, Comparison of n-γ discrimination by zero-crossing and digital charge comparison methods, Nuclear Instruments and Methods in Physics Research Section A: Accelerators, Spectrometers, Detectors and Associated Equipment 360 (3) (1995) 584 – 592. doi:10.1016/0168-9002(95)00037-2.

[23] D. I. Shippen, M. J. Joyce, M. D. Aspinall, A wavelet packet transform inspired method of neutron-gamma discrimination, IEEE Transactions on Nuclear Science 57 (5) (2010) 2617–2624. doi:10.1109/TNS.2010.2044190.

[24] K. A. A. Gamage, M. J. Joyce, N. P. Hawkes, A comparison of four different digital algorithms for pulse-shape discrimination in fast scintillators, Nuclear Instruments and Methods in Physics Research, Section A: Accelerators, Spectrometers, Detectors and Associated Equipment 642 (1) (2011) 78–83. doi:10.1016/j.nima.2011.03.065.

[25] S. W. Smith, The Scientist and Engineer's Guide to Digital Signal Processing, Second Edition, California Technical Publishing, San Diego, 1999.

[26] B. D'Mellow, M. D. Aspinall, R. O. Mackin, M. J. Joyce, A. J. Peyton, Digital discrimination of neutrons and γ-rays in liquid scintillators using pulse gradient analysis, Nuclear Instruments and Methods in Physics Research, Section A: Accelerators, Spectrometers, Detectors and Associated Equipment 578 (1) (2007) 191–197. doi:10.1016/j.nima.2007.04.174.

[27] M. J. Joyce, M. D. Aspinall, F. D. Cave, A. Lavietes, A 16-channel real-time digital processor for pulse-shape discrimination in multiplicity assay, IEEE Transactions on Nuclear Science 61 (4) (2014) 2222–2227. doi:10.1109/TNS.2014.2322574.

[28] M. J. Balmer, K. A. Gamage, G. C. Taylor, Comparative analysis of pulse shape discrimination methods in a ^{6}Li loaded plastic scintillator, Nuclear Instruments and Methods in Physics Research Section A: Accelerators, Spectrometers, Detectors and Associated Equipment 788 (2015) 146–153. doi:10.1016/j.nima.2015.03.089.

[29] M. Flaska, M. Faisal, D. D. Wentzloff, S. A. Pozzi, Influence of sampling properties of fast-waveform digitizers on neutron-gamma-ray, pulse-shape discrimination for organic scintillation detectors, Nuclear Instruments and Methods in Physics Research, Section A: Accelerators, Spectrometers, Detectors and Associated Equipment 729 (2013) 456–462. doi:10.1016/j.nima.2013.07.008.

[30] M. J. I. Balmer, K. A. A. Gamage, G. C. Taylor, A novel approach to neutron dosimetry, Medical Physics 43 (11) (2016) 5981–5990. doi:10.1118/1.4964456.

[31] S. A. Pozzi, M. M. Bourne, S. D. Clarke, Pulse shape discrimination in the plastic scintillator EJ-299-33, Nuclear Instruments and Methods in Physics Research, Section A: Accelerators, Spectrometers, Detectors and Associated Equipment 723 (2013) 19–23. doi:10.1016/j.nima.2013.04.085.

[32] M. M. Bourne, J. Whaley, J. L. Dolan, J. K. Polack, M. Flaska, S. D. Clarke, A. Tomanin, P. Peerani, S. A. Pozzi, Cross-correlation measurements with the EJ-299-33 plastic scintillator, Nuclear Inst. and Methods in Physics Research, A 806 (2016) 348–355. 10.1016/j.nima.2014.10.052.

[33] Inrad Optics, Stilbene Single Crystals, Data sheet.

[34] M. Aspinall, B. D'Mellow, R. Mackin, M. Joyce, N. Hawkes, D. Thomas, Z. Jarrah, A. Peyton, P. Nolan, A. Boston, Verification of the digital discrimination of neutrons and rays using pulse gradient analysis by digital measurement of time of flight, Nuclear Instruments and Methods in Physics Research Section A: Accelerators, Spectrometers, Detectors and Associated Equipment 583 (2–3) (2007) 432 – 438. doi:10.1016/j.nima.2007.09.041.

[35] R. Gehrke, R. Aryaeinejad, J. Hartwell, W. Yoon, E. Reber, J. Davidson, The γ-ray spectrum of ^{252}Cf and the information contained within it, Nuclear Instruments and Methods in Physics Research Section B: Beam Interactions with Materials and Atoms 213 (2004) 10 – 21. doi:10.1016/S0168-583X(03)01526-X.

[36] T. E. Valentine, Evaluation of prompt fission gamma rays for use in simulating nuclear safeguard measurements, Annals of Nuclear Energy 28 (3) (2001) 191 – 201. doi:10.1016/S0306-4549(00)00039-6.

[37] M. J. Cieślak, K. A. Gamage, R. Glover, Coded-aperture imaging systems: Past, present and future development – a review, Radiation Measurements 92 (2016) 59 – 71. doi:10.1016/j.radmeas.2016.08.002.

[38] J. K. Polack, M. Flaska, A. Enqvist, C. S. Sosa, C. C. Lawrence, S. A. Pozzi, An algorithm for charge-integration, pulse-shape discrimination and estimation of neutron/photon misclassification in organic scintillators, Nuclear Instruments and Methods in Physics Research, Section A: Accelerators, Spectrometers, Detectors and Associated Equipment 795 (2015) 253–267. doi:10.1016/j.nima.2015.05.048.

[39] M. Cieslak, K. Gamage, Design and development of a real-time readout electronics system to retrieve data from a square multi-anode photomultiplier tube for neutron gamma pulse shape discrimination, in: 2016 IEEE-NPSS Real Time Conference (RT), 2016, pp. 1–4. doi:10.1109/RTC.2016.7543129.

[40] Eljen Technology, EJ-299-33A, EJ-299-34, Data sheet.

[41] John D. Hunter, Matplotlib: A 2D Graphics Environment, Computing in Science & Engineering, 9, 2007, 90-95. doi:10.1109/MCSE.2007.55.